

Evaporation Reduction by Windbreaks: Overview, Modelling and Efficiency

Fernanda Helfer, Hong Zhang and Charles Lemckert

November 2009



Urban Water Security Research Alliance
Technical Report No. 16

Urban Water Security Research Alliance Technical Report ISSN 1836-5566 (Online)

Urban Water Security Research Alliance Technical Report ISSN 1836-5558 (Print)

The Urban Water Security Research Alliance (UWSRA) is a \$50 million partnership over five years between the Queensland Government, CSIRO's Water for a Healthy Country Flagship, Griffith University and The University of Queensland. The Alliance has been formed to address South-East Queensland's emerging urban water issues with a focus on water security and recycling. The program will bring new research capacity to South-East Queensland tailored to tackling existing and anticipated future issues to inform the implementation of the Water Strategy.

For more information about the:

UWSRA - visit <http://www.urbanwateralliance.org.au/>

Queensland Government - visit <http://www.qld.gov.au/>

Water for a Healthy Country Flagship - visit www.csiro.au/org/HealthyCountry.html

The University of Queensland - visit <http://www.uq.edu.au/>

Griffith University - visit <http://www.griffith.edu.au/>

Enquiries should be addressed to:

The Urban Water Security Research Alliance

PO Box 15087

CITY EAST QLD 4002

Ph: 07-3247 3005; Fax: 07-3405 3556

Email: Sharon.Wakem@qwc.qld.gov.au

Citation: Helfer, F, Zhang, H. and Lemckert, C. J. (2009). *Evaporation Reduction by Windbreaks: Overview, Modelling and Efficiency*. Urban Water Security Research Alliance Technical Report No. 16.

Copyright

© 2009 Griffith University. To the extent permitted by law, all rights are reserved and no part of this publication covered by copyright may be reproduced or copied in any form or by any means except with the written permission of Griffith University.

Disclaimer

The partners in the UWSRA advise that the information contained in this publication comprises general statements based on scientific research and does not warrant or represent the accuracy, currency and completeness of any information or material in this publication. The reader is advised and needs to be aware that such information may be incomplete or unable to be used in any specific situation. No action shall be made in reliance on that information without seeking prior expert professional, scientific and technical advice. To the extent permitted by law, UWSRA (including its Partner's employees and consultants) excludes all liability to any person for any consequences, including but not limited to all losses, damages, costs, expenses and any other compensation, arising directly or indirectly from using this publication (in part or in whole) and any information or material contained in it.

Cover Photograph:

From CSIRO's ScienceImage: www.scienceimage.csiro.au

File:EM7349.jpg

Description: View over Maroondah Reservoir, near Healesville, Victoria

Photographer: Nick Pitsas

© 2008 CSIRO

FOREWORD

Water is fundamental to our quality of life, to economic growth and to the environment. With its booming economy and growing population, Australia's South-East Queensland (SEQ) region faces increasing pressure on its water resources. These pressures are compounded by the impact of climate variability and accelerating climate change.

The Urban Water Security Research Alliance, through targeted, multidisciplinary research initiatives, has been formed to address the region's emerging urban water issues.

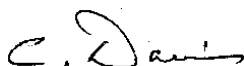
As the largest regionally focused urban water research program in Australia, the Alliance is focused on water security and recycling, but will align research where appropriate with other water research programs such as those of other SEQ water agencies, CSIRO's Water for a Healthy Country National Research Flagship, Water Quality Research Australia, eWater CRC and the Water Services Association of Australia (WSAA).

The Alliance is a partnership between the Queensland Government, CSIRO's Water for a Healthy Country National Research Flagship, The University of Queensland and Griffith University. It brings new research capacity to SEQ, tailored to tackling existing and anticipated future risks, assumptions and uncertainties facing water supply strategy. It is a \$50 million partnership over five years.

Alliance research is examining fundamental issues necessary to deliver the region's water needs, including:

- ensuring the reliability and safety of recycled water systems.
- advising on infrastructure and technology for the recycling of wastewater and stormwater.
- building scientific knowledge into the management of health and safety risks in the water supply system.
- increasing community confidence in the future of water supply.

This report is part of a series summarising the output from the Urban Water Security Research Alliance. All reports and additional information about the Alliance can be found at <http://www.urbanwateralliance.org.au/about.html>.



Chris Davis
Chair, Urban Water Security Research Alliance

CONTENTS

Foreword	i
1. Introduction	1
2. Mechanism for Reducing Evaporation	1
3. Commercially Available Products.....	2
4. Review of Existing Studies.....	2
4.1. Influence of Windbreaks on Wind Speed	3
4.2. Influence of Windbreaks on Evaporation	7
5. Modelling Analysis	7
5.1. Study Domain	7
5.2. Model Description	7
5.2.1. Daily Evaporation Estimate	8
5.2.2. Wind Modelling	10
5.2.3. Boundary Conditions	10
5.2.4. Windbreak Effect Inclusions	12
6. Modelling Results.....	13
7. Cost Efficiency	15
8. Key Messages.....	16
9. Conclusion	16
References	17

LIST OF FIGURES

Figure 1:	Windbreak system showing the quiet and wake zones created downwind and expected wind speed reduction on the leeward side of the barrier (Hipsey, 2002)	2
Figure 2:	Estimated wind reduction in the up and downwind sides of a permeable windbreak (adapted from van Eimern <i>et al.</i> , 1964)	3
Figure 3:	Estimated reduction in daily potential evapotranspiration on the windward and leeward sides of a permeable windbreak (Pryor and Nadler, 2006)	4
Figure 4:	Wind speed reductions on the lee side of windbreaks with different densities (adapted from Brandle and Finch, 1991)	4
Figure 5:	Vertical profiles of wind speed at varying locations around a single, medium porosity windbreak (Judd <i>et al.</i> , 1996 presented by Cleugh, 1998)	5
Figure 6:	Vertical profiles of wind speed measured around a single, medium porosity windbreak. The scale for the wind speed profiles is normalised – u is the actual wind speed measured at various heights (z) and downwind locations (marked beside each profile, in windbreak heights) and u_o is the upwind wind speed measured at $z = 4$ m (Bradley and Mulhearn, 1983 presented by Cleugh, 1998). NB In this study $h=H$	5
Figure 7:	Horizontal profiles of wind speed for windbreaks with varying porosity (Wang and Takle, 1997a presented by Cleugh, 1998)	5
Figure 8:	Wind speed produced by various shelter shapes, normalised by the upstream undisturbed wind speed. HH, AA, AL, AJ, SA, SL, SJ are labels for shelterbelt shapes (adapted from Wang and Takle, 1997b)	6
Figure 9:	Spatial pattern of average U/U_o derived from cup anemometer measurements (Cleugh, 2002)	6
Figure 10:	Map of Wivenhoe Dam (Yao <i>et al.</i> , 2009).....	8
Figure 11:	Examples of wind speed profiles in a boundary layer (Oke, 1978 presented by Yao, 2008).....	11
Figure 12:	Horizontal profiles of wind speed on the leeward side of windbreaks with different heights (adapted from the works of van Eimern <i>et al.</i> , 1964; Bradley and Mulhearn, 1983; Brandle and Finch, 1991; Wang and Takle, 1995a; Hipsey <i>et al.</i> , 2004 and Brandle <i>et al.</i> , 2004)	12
Figure 13:	Hypothetical shape of Wivenhoe Dam for the simulations.....	13
Figure 14:	Calculated annual evaporation rate on the leeward side of windbreaks with different heights at Wivenhoe Dam in 2007	14
Figure 15:	Estimated annual wind speed reductions on the leeward side of windbreaks with different heights at Wivenhoe Dam in 2007.....	15

LIST OF TABLES

Table 1:	Estimated monthly evaporation rates for different windbreak protection scenarios along the wind fetch ¹ of Wivenhoe Dam in 2007 (mm)	13
Table 2:	Summary of the results of the simulations on Wivenhoe Dam during 2007.....	14

1. INTRODUCTION

This report has been prepared for the Urban Water Security Research Alliance for the purposes of assessing the potential for windbreaks to reduce evaporation from water storages in South East Queensland (SEQ). This report forms one of a group of reports, each of which assesses the applicability of different evaporation mitigation techniques to SEQ water supply systems.

2. MECHANISM FOR REDUCING EVAPORATION

Water evaporation is a process that depends on wind speed and the humidity gradient between the water surface and the air above. The humidity gradient is determined by the dryness of the air and the temperature. Windbreaks reduce evaporation by limiting the volume of hot air passing over the warm water surface. A moisture blanket over the water surface develops from a reduction in the rate at which moisture is removed from the water surface. The development of this moist layer acts to further reduce evaporation by reducing the humidity gradient between the water surface and the overlaying air.

Additionally, windbreaks can contribute to reducing evaporation by humidifying the air passing through the trees due to their transpiration, and then enhancing the moisture blanket over the water surface and decreasing the humidity gradient. Furthermore, decreasing effective wind speed will reduce the size and number of waves generated on the water surface, therefore minimising the area in contact with the atmosphere, restricting the potential of the evaporation process.

Due to practical difficulties, understanding of the influence of windbreaks on evaporation of large open waters is limited. Few studies have been undertaken into the effect of windbreaks on evaporation from small water bodies (Skidmore and Hagen, 1970; Lomas and Schlesinger, 1971; Messing *et al.*, 1998; Hipsey and Sivapalan, 2003; Hipsey *et al.*, 2004).

Some studies have been undertaken on the application of windbreaks in agriculture, where the main effects of windbreaks on crop growth and production were assessed (Brown and Rosenberg, 1971; Cleugh, 1998; Wang and Takle, 1998; Cleugh *et al.*, 2002; Brandle *et al.*, 2004). The effect of shelterbelts on meteorological variables the wind speed and temperature were examined by Rosenberg (1966), Raine and Stevenson (1977), McNaughton (1988), Heisler and Dewalle (1988), Cleugh (1998; 2002), Wang *et al.* (2001), Sudmeyer and Scott (2002) and others. The benefits of using windbreaks in agriculture are connected to their potential to reduce wind speed. Advantages include reduction of direct mechanical effects of wind on plants, erosion, sandblasting, burial of seeds and dissemination of pests, pathogens and pollutants. As evaporation depends on air movement, the reduction of wind speed caused by windbreaks may reduce the evaporation rate in certain areas downwind of the barrier.

The efficiency of a windbreak on wind speed reduction depends mainly on its permeability, height and orientation in relation to the prevailing wind (Hipsey, 2002; Wilson and Josiah, 2004; Heisler and Dewalle, 1988; Brandle *et al.*, 2004; FAO, 1989; Brandle and Finch, 1991; Cleugh, 1998; Cleugh *et al.*, 2002; Wang *et al.* 2001). If the barrier is dense (like a solid wall) the airflow will pass over its top and cause turbulence on the leeward side due to lower pressure on this side, thus providing a limited zone of effective shelter on the leeward side compared with the zone created by a moderately permeable shelter (FAO, 1989).

Optimum permeability for maximum wind speed reduction varies from 40 to 50 per cent of open space, corresponding with a density of 50 to 60 per cent in vegetation (Wang *et al.*, 2001; Brandle and Finch, 1991; FAO, 1989; Heisler and Dewalle, 1988; Hipsey, 2002). It is expected that the barrier will have some influence on the wind speed over a distance up to 30 times its height (H) on the leeward side, with a maximum effect expected over an area of 5 H (Brandle and Finch, 1991; Wang and Takle, 1995a; Wang and Takle, 1995b; Brandle *et al.*, 2004; Pryor and Nadler, 2006). Maximum effectiveness will be established if the barrier is placed perpendicularly to the direction of the prevailing wind (FAO, 1989; Wilson and Josiah, 2004, Hipsey, 2002). Narrow barriers have been shown to be as effective as wide ones for reducing wind speed (FAO, 1989). Wang and Takle (1997b) verified there are insignificant differences in wind speed reduction between shelterbelts of different shapes.

The objective of this study was to analyse the effects of windbreaks on wind speed and to assess whether they could be effective as a mechanism for reducing evaporation from large reservoirs in South East Queensland. Three different heights of windbreak trees (20, 30 and 40m) were examined by employing desktop modelling techniques. In order to simplify this analysis, all barriers were assumed to have the same porosity (medium density), and to be placed perpendicularly to the prevailing wind direction.

3. COMMERCIALY AVAILABLE PRODUCTS

There is a wide range of tree species that can be used as windbreaks. Volume of water used, suitability to soil type, impacts on water quality, lateral root growth, foliage density and growth rate are some of the aspects to be considered. A combination of species is also recommended to maximise foliage uniformity and biodiversity (Hipsey, 2002). Conifer trees (pines), species of acacia and eucalypts are common types of trees used for windbreak design (Wilson and Josiah, 2004). Pines can grow from three to 80m tall, with the majority of species reaching between 15-45m tall when mature (Australian Flora Resources Database). Eucalypts can reach up to 60m, with the common size being 20 to 40m (Australian Flora Resources Database).

4. REVIEW OF EXISTING STUDIES

A windbreak provides shelter from the wind and, in doing so, alters wind speed, wind direction and airflow turbulence, thus indirectly influencing the evaporation process for some distance downwind of the shelter itself. The downwind distance under influence by the shelter depends on the nature of the windbreak (e.g. artificial barrier or tree shelter belt); its density (or porosity); orientation to the wind (or wind direction); and, particularly, its height (Hipsey, 2002; Brandle and Finch, 1991; Cleugh, 1998; Cleugh *et al.*, 2002; Wang *et al.*, 2001).

The works of Raine and Stevenson (1977), Bradley and Mulhearn (1983), Brandle and Finch (1991), Wang and Takle (1995a), Hipsey *et al.* (2004), Brandle *et al.* (2004), Pryor and Nadler (2006) and many others describe how wind behaves downwind from shelterbelts. There is a *quiet zone* just behind the barrier over which the wind speed is significantly reduced. Its length is generally assumed to range between 5 H and 10 H. Further downwind, beyond the quiet zone, the airflow gradually recovers to its upwind speed within the *turbulent wake zone*, which extends up to a distance of 30 H. Figure 1 presents a sketch of how wind behaves on the leeward side of a windbreak, within the quiet and wake zones.

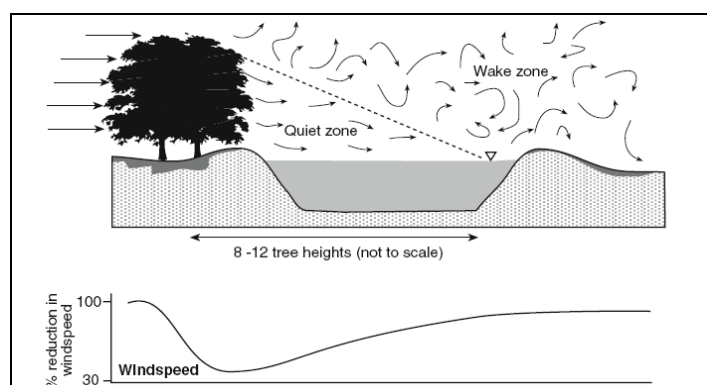


Figure 1: Windbreak system showing the quiet and wake zones created downwind and expected wind speed reduction on the leeward side of the barrier (Hipsey, 2002)

Although studies detailing the direct application of windbreaks to reduce open water evaporation are limited, many other studies have investigated the influence of windbreaks on wind speed and turbulence behind the barrier, and have quantified the reduction in wind velocity downwind and upwind from the windbreak. Most of these works have derived data from experimentation, conducted either in wind tunnels or over flat fields using short fences.

4.1. Influence of Windbreaks on Wind Speed

Windbreaks present an obstacle to the wind. Over the windbreak top (where $z/H > 1$, with z being height above the ground), the wind is deflected upward and the streamlines of the flow are compressed. Below the barrier top ($z/H < 1$), the wind is reduced to zero behind a solid barrier, and to intermediate speeds at more open barriers where some wind can pass through the structure (McNaughton, 1988). Therefore, a zone of strong wind velocity occurs just above the top of a windbreak. This widens and follows the streamline as the air moves downwind and acts as a source of turbulent kinetic energy (Finnigan and Bradley, 1983). The wind speed is lower next to the ground, and it remains slow over a great distance (McNaughton, 1988).

The shelter effect is most often represented by the distance over which a shelterbelt reduces wind speed by a given significant percentage (commonly 80%) and by the minimum wind speed (maximum wind reduction) and its location (Wang and Takle, 1997b). Reductions in wind speed have been recorded as far as 50 H to the leeward side of windbreaks; however, only small and insignificant reductions have been found further down from 25 H (Heisler and Dewalle, 1988; Condie and Webster, 1995). From the majority of the research carried out on windbreaks and wind speed, it can be accepted that the influence of shelterbelts on wind velocity extends up to a distance of 30 H, with maximum influence taking place at 5 H (van Eimern *et al.*, 1964; Bradley and Mulhearn, 1983; Wang and Takle, 1995a; Brandle and Finch, 1991; Hipsey *et al.*, 2004; Brandle *et al.*, 2004).

Figure 2 presents the wind speed reduction downwind compared with upwind for a moderately dense shelter (50 to 70 per cent optical porosity).

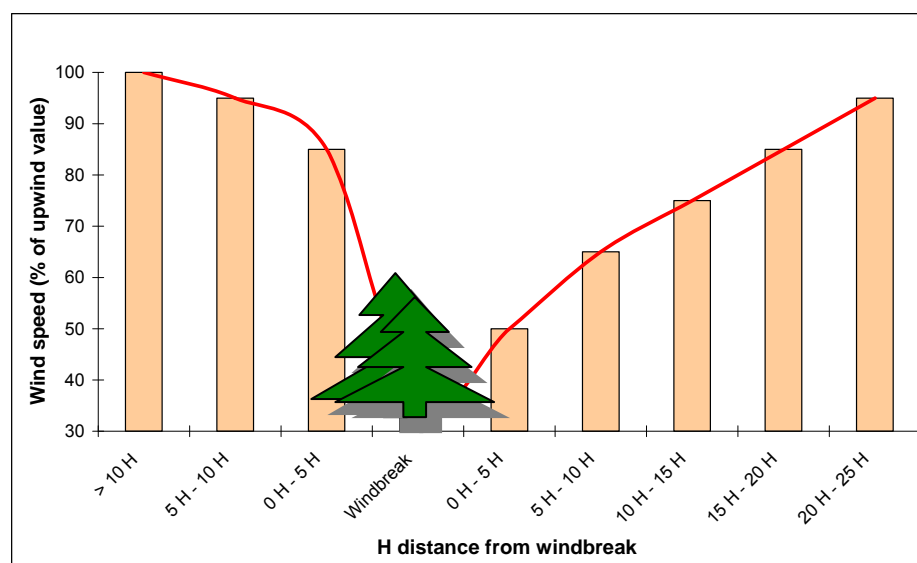


Figure 2: Estimated wind reduction in the up and downwind sides of a permeable windbreak (adapted from van Eimern *et al.*, 1964)

Figure 2 shows the estimated reduction in wind speed at $z = 0.5 H$, resulting from the use of a permeable windbreak (van Eimern *et al.*, 1964). The area adjacent to the shelter, extending out to approximately 5 H of the shelter, experiences a 50 per cent reduction in wind speed. Pryor and Nadler (2006), examining the microclimate effects in field crop production, concluded that this reduction would cause the rate of daily potential evapotranspiration to decline to about 84% of that expected further from the windbreak (Figure 3).

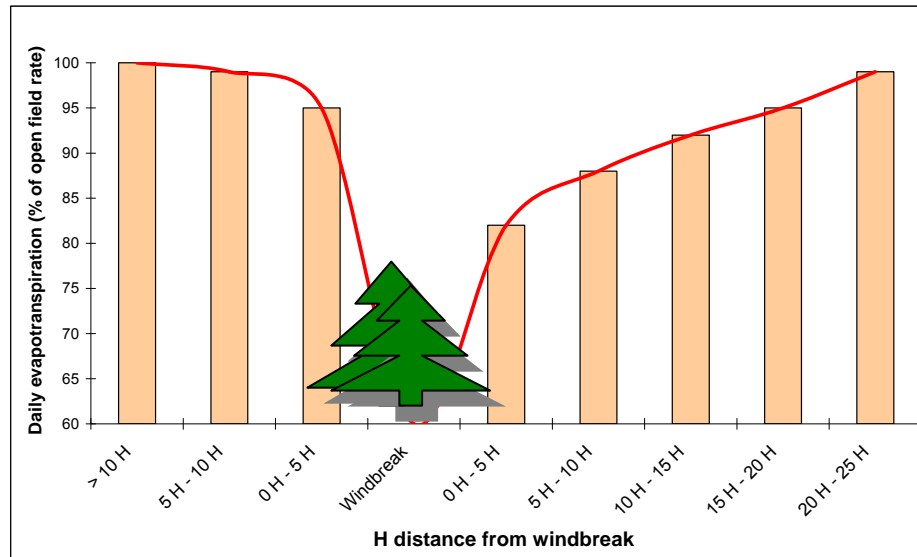


Figure 3: Estimated reduction in daily potential evapotranspiration on the windward and leeward sides of a permeable windbreak (Pryor and Nadler, 2006)

Brandle and Finch (1991) investigated how windbreak density affects wind flow patterns at different extents downwind. Around very dense windbreaks, air pressure increases on the windward side, while a low pressure zone develops on the leeward side. The windward air pressure pushes air through and over the windbreak, while the leeward low pressure area behind it pulls air coming over the windbreak downwind. If the windbreak is very dense, the flow in the quiet zone can reverse direction to form a recirculating eddy (Cleugh, 1998). As windbreak density decreases, the volume of air passing through the barrier increases, reducing the pressure differences between the upwind and downwind sides. This results in a longer protected area downwind. In general, different wind speed patterns and sheltered areas can be established by adjusting windbreak density (Figure 4).

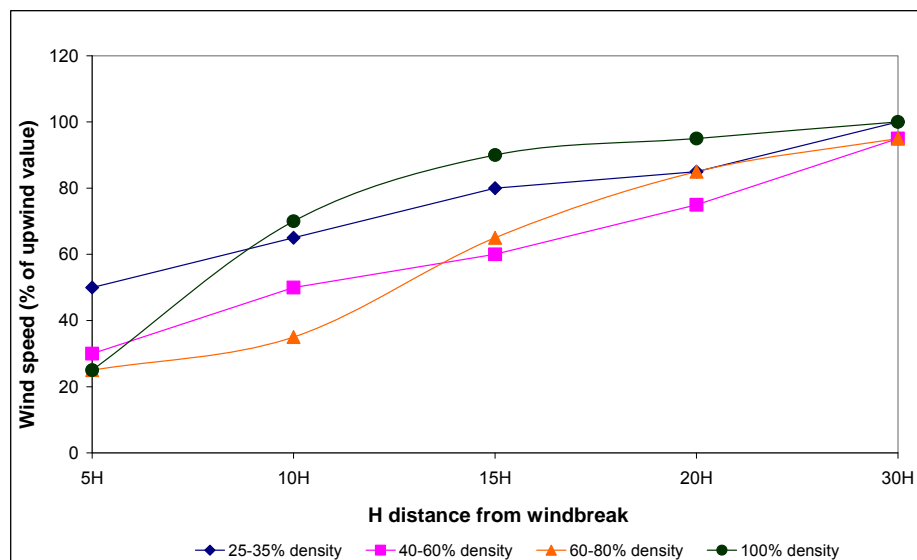


Figure 4: Wind speed reductions on the lee side of windbreaks with different densities (adapted from Brandle and Finch, 1991)

Based on existing wind tunnel experiments, field observations and numerical modelling, Cleugh (1998) addressed the influence of porous windbreaks on the airflow pattern, microclimate and crop yields. Profiles of wind speed measured at several locations upwind and downwind from a medium porosity windbreak were obtained from a wind tunnel experiment initially performed by Judd *et al.* (1996). The resulting outcomes, as shown in Figure 5, are typical of what might be seen over an extensive, uniform wheat crop (Cleugh, 1998).

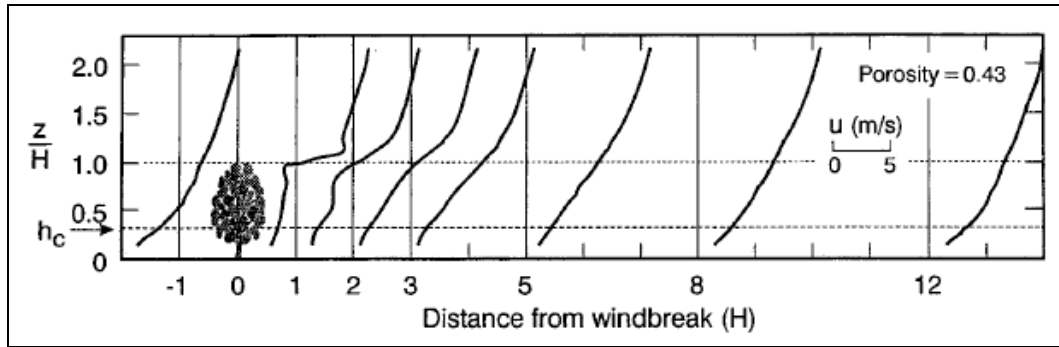


Figure 5: Vertical profiles of wind speed at varying locations around a single, medium porosity windbreak (Judd *et al.*, 1996 presented by Cleugh, 1998)

The wind speed profiles found in Judd *et al.* (1996) are similar to those found by Bradley and Mulhearn (1983), cited by Cleugh (1998). In the latter, the profiles were measured around a shelter fence (porosity = 0.5) placed in a bare field (Figure 6). Three trends of wind speed downwind from the windbreaks can be noted: (a) accelerating flow over the top of the windbreak; (b) lower wind speeds immediately behind the windbreak; and (c) some acceleration through the plant canopy at the base of the windbreak.

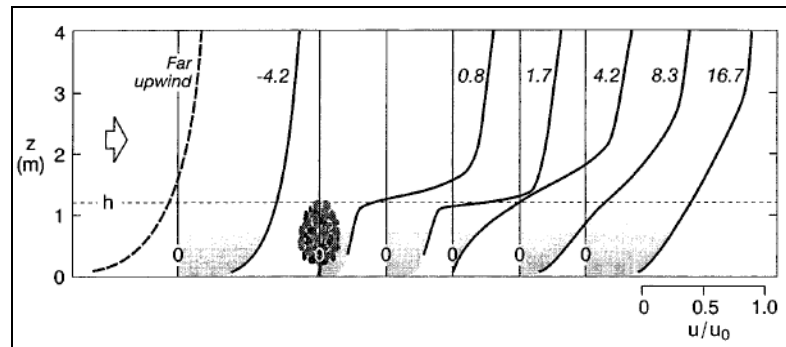


Figure 6: Vertical profiles of wind speed measured around a single, medium porosity windbreak. The scale for the wind speed profiles is normalised – u is the actual wind speed measured at various heights (z) and downwind locations (marked beside each profile, in windbreak heights) and u_0 is the upwind wind speed measured at $z = 4\text{ m}$ (Bradley and Mulhearn, 1983 presented by Cleugh, 1998). NB In this study $h=H$.

Figure 7 shows the spatial variation of average horizontal wind speed for windbreaks with varying porosity (Wang and Takle, 1997a cited by Cleugh, 1998). The wind speed was measured at a height below $0.5 H$, and was expressed as a percentage of the upwind wind speed. Maximum reductions between $2 H$ and $8 H$ (depending on porosity) and around 80 per cent recovery of the upwind wind velocity at about $20 H$ were found.

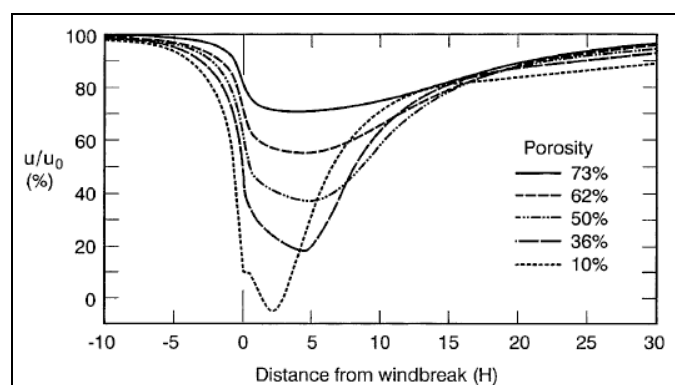


Figure 7: Horizontal profiles of wind speed for windbreaks with varying porosity (Wang and Takle, 1997a presented by Cleugh, 1998)

The results of the work of Wang and Takle (1997b), who studied the influences of shelterbelt shapes on wind-sheltering efficiency by numerical modelling have been summarised in Figure 8. The measurements of wind speed presented on the graph were taken at $z = 0.5 H$.

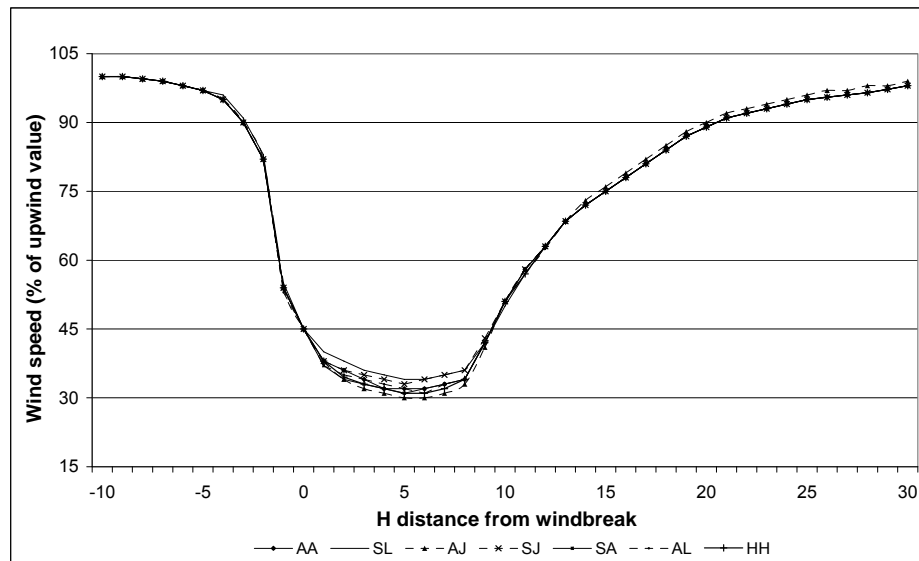


Figure 8: Wind speed produced by various shelter shapes, normalised by the upstream undisturbed wind speed. HH, AA, AL, AJ, SA, SL, SJ are labels for shelterbelt shapes (adapted from Wang and Takle, 1997b)

According to the results of the simulation, locations where minimum wind speeds occur are closer to the windbreak for higher z values, and farther from the windbreak for lower z values. It was also found that there are only small differences in wind speed reduction by shelterbelts of different shapes, and that the effect of shelterbelt shape on the shelter distance is negligible.

Cleugh (2002) conducted a field experiment program to quantify the effect of windbreaks on the microclimate and evaporation fluxes at a tree windbreak site located in South East Australia. The study revealed that a broad zone of reduced wind speeds extended from $1 H$ to $5 H - 6 H$. Figure 9 presents these findings and illustrates the variation in the ratio of the near surface ($z = 0.3 H$), horizontal wind speed measured downwind ($U(X)$), and upwind (U_0) from the windbreak.

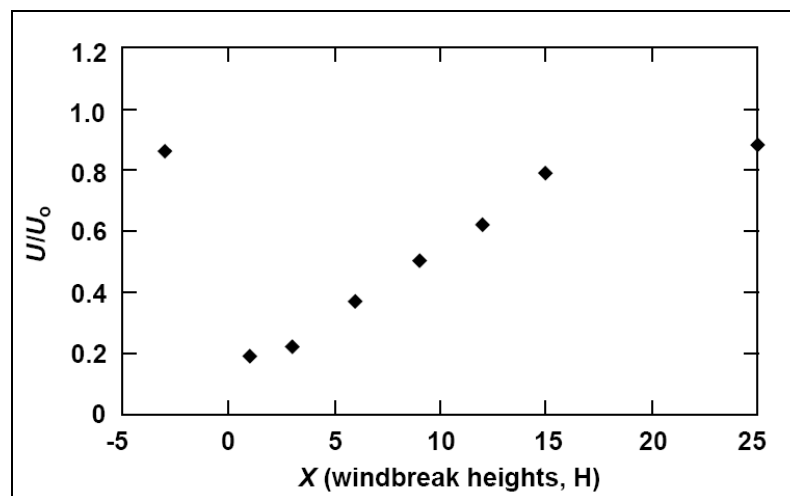


Figure 9: Spatial pattern of average U/U_0 derived from cup anemometer measurements (Cleugh, 2002)

4.2. Influence of Windbreaks on Evaporation

The effect of windbreaks on evaporation have been previously detailed by Skidmore and Hagen (1970), Lomas and Schlesinger (1971), Miller *et al.* (1973), Messing *et al.* (1998), Hipsey *et al.* (2004) and others. Skidmore and Hagen (1970), Lomas and Schlesinger (1971) and Messing *et al.* (1998) have documented that evaporation can be reduced by up to 35% on the leeward side of the windbreak barriers, and that evaporative reductions are proportional to decreases in wind speed. Miller *et al.* (1973) reported that during six days of measurements a mean 20% decrease in evaporation on the leeward side of a shelter was seen. In China, regional evaporation was reduced by 14% across a large-scale shelterbelt network (Wang *et al.*, 2001). Hipsey *et al.* (2004) found a reduction of approximately 30% in evaporation from small dams (approximately 3,600m² in area) placed downwind of an 8m high tree windbreak.

The effect of windbreaks on evaporation is complicated by turbulence induced by the barrier, and thus is difficult to simulate (Wang and Takle, 1995a; Wang and Takle, 1995b; Wang *et al.*, 2001). When modelling evapotranspiration in wet soil conditions, these authors found that evapotranspiration is significantly reduced during daytime in an area as far as 25 H. A maximum reduction of 50% in evapotranspiration occurs between 4 - 7 H, where reductions of wind and turbulence also reach their maxima. When analysing the effects of windbreaks' density on evapotranspiration using modelling, they found that very dense barriers cause recirculation and separation of wind streamlines on the near leeward side leading to the diminishing reduction of evapotranspiration by the shelter. It was concluded that maximum reductions in evaporation can be obtained from medium-density shelters.

5. MODELLING ANALYSIS

5.1. Study Domain

The following study was carried out on the Wivenhoe Dam (27.4944 S, 152.6889 E), built on the Brisbane River (Figure 10), and was chosen for model assessment due to availability of suitable data and to keep consistent with the work of McJannet *et al.* (2008a). The Wivenhoe Dam surface area and water storage data was provided by Seqwater. At full supply level (67m above sea level), Wivenhoe Dam has a surface area of 107.5 km² and a capacity of 1,165,238 ML (Seqwater). Its average width at full supply level is about 2 km, and its average depth is 25m (Yao, 2008).

5.2. Model Description

In order to simulate the influence of windbreaks on evaporation, the numerical model developed by Yao (2008) was modified to include the reduction of wind speed due to the hypothetical presence of a barrier located upwind of the wind fetch.

The model developed by Yao (2008) is based on the Penman-Monteith (PM) equation (Monteith, 1965), whose terms are described by Jensen *et al.* (1990). The required meteorological data consist of: incoming solar radiation; vapour pressure at 2m height; air temperature at 2m height; and wind speed at 10m height. The model defined by Yao (2008) also includes the evolution of wind speed, vapour pressure and air temperature over the water surface in order to increase output precision (Beletsky and Schwab, 2001; Schwab and Morton, 1984; cited by Yao, 2008). Additionally, Yao (2008) incorporated the water body temperature profile into the model in order to better estimate the surface water temperature. The surface water temperature serves as a boundary condition influencing the profile of vapour pressure and air temperature, and consequently the evaporation.

The period of simulation used in this analysis ran from January 2007 to January 2008. The meteorological data sets required by the model were obtained from University of Queensland Gatton station (site no. 040082) located about 35 km away from Wivenhoe Dam.

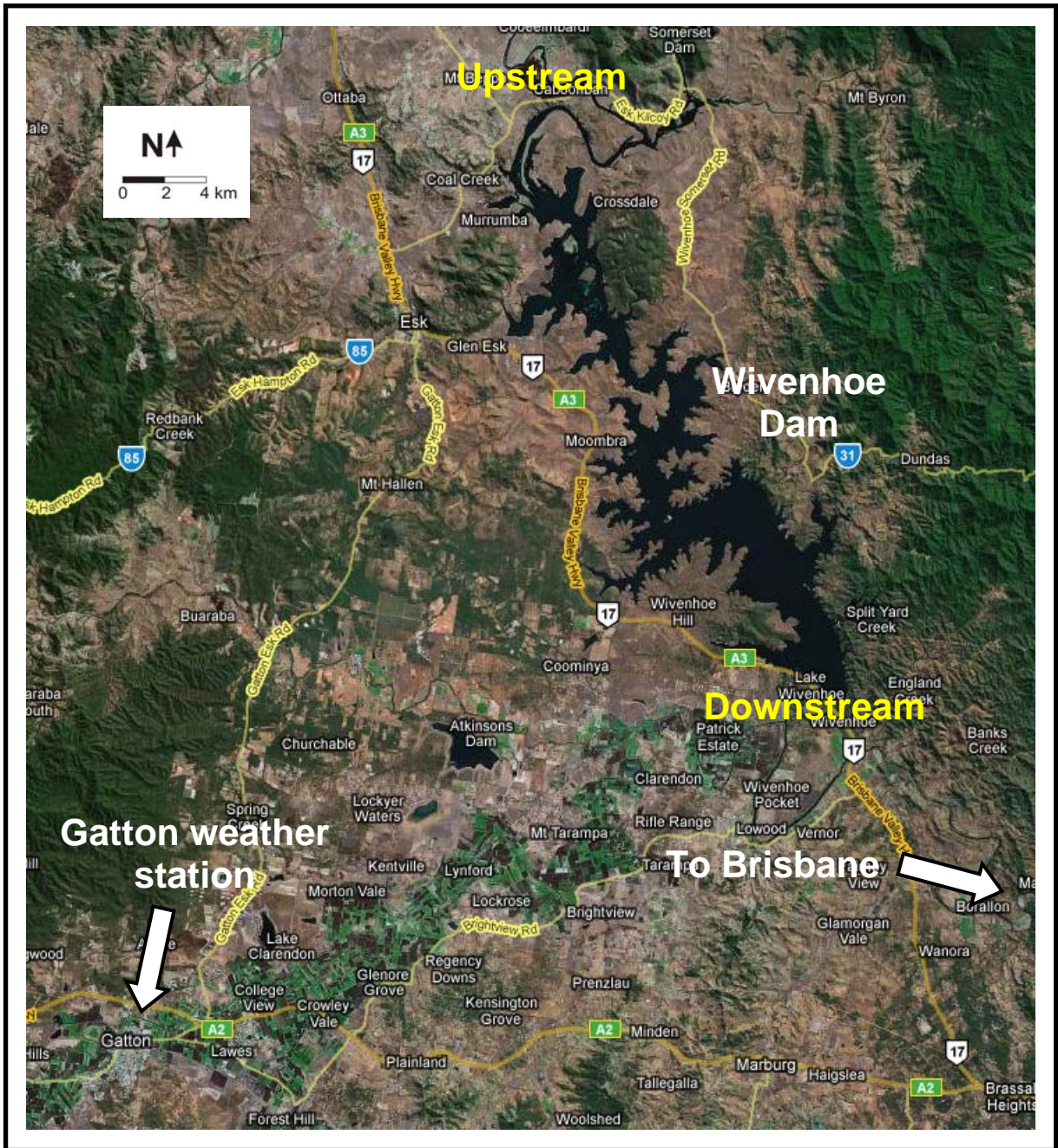


Figure 10: Map of Wivenhoe Dam (Yao *et al.*, 2009)

5.2.1. Daily Evaporation Estimate

The daily evaporation rate from Wivenhoe Dam was calculated using the PM equation (Monteith, 1965). As discussed above, in order to solve this equation, four sets of meteorological data are required: incoming solar radiation; vapour pressure at 2m height ($z = 2\text{m}$); air temperature at 2m height ($z = 2\text{m}$) and wind speed at 10m height ($z = 10\text{m}$).

The meteorological data used in this work is the same as that used by Yao (2008), and was sourced from the University of Queensland Gattton station (site number 040082; 27.5436 S, 152.3375 E). The station's elevation was assumed to be the same as the water surface of Wivenhoe Dam, while wind speed was measured at 10m above ground, and temperature and vapour pressure were measured at 1.2m height. For simplicity, when entering the PM equation, these two sets of data were assumed to be equal to those measured at 2m above ground.

The PM equation is given by:

$$E = \frac{1}{\lambda} \left(\frac{\Delta_w (Q^* - N) + 86400 \rho_a c_a (P_{vw}^* - P_v) / r_a}{\Delta_w + \gamma} \right) \quad (1)$$

where E (mm.d^{-1}) is the daily evaporation rate; λ (MJ.Kg^{-1}) is the latent heat of vaporisation; Δ_w ($\text{kPa}^\circ\text{C}^{-1}$) is the slope of the temperature saturation water vapour curve at surface water temperature; T_{ws} ($^\circ\text{C}$); Q^* ($\text{MJ.m}^{-2}.\text{d}^{-1}$) is the net radiation; N ($\text{MJ.m}^{-2}.\text{d}^{-1}$) is the change of heat storage in the water body; ρ_a (Kg.m^{-3}) is the air density; c_a ($\text{MJ.Kg}^{-1}.\text{K}^{-1}$) is the specific heat of air; P_{vw}^* (kPa) is the saturated vapour pressure at water temperature; P_v (kPa) is the vapour pressure overwater; r_a (s.m^{-1}) is the aerodynamic resistance; and γ ($\text{kPa}^\circ\text{C}^{-1}$) is the psychometric constant. The derivation of each parameter in the PM equation is described in detail by Yao (2008).

According to the definition for r_a , given by Calder and Neal (1984), the PM equation can be re-written as:

$$E = k_1 (Q^* - N) + k_2 f(u) (P_{vw}^* - P_v) \quad (2)$$

where:

$$k_1 = \frac{\Delta_w}{(\Delta_w + \gamma)\lambda} \quad (3)$$

$$k_2 = \frac{\gamma}{(\Delta_w + \gamma)\lambda} \quad (4)$$

and $f(u)$ is a wind function dependent upon the area of the water body and wind speed overland at 10m height. For the purposes of this study, the wind function used here is the equation presented by McJannet *et al.* (2008a) and applied by McJannet *et al.* (2008b):

$$f(u) = A^{-0.05} (6.79 + 1.57u_{(10)}) \quad (5)$$

where $u_{(10)}$ is the wind speed at 10m height, and A is the surface area of the reservoir in m^2 . It is important to note that this function is different to that one applied by Yao (2008).

It can be seen that the PM equation has two distinct parts. The first term ($k_1(Q^*-N)$) is an energy balance term, while the second ($k_2f(u)(P_{vw}^*-P_v)$), is an aerodynamic term. Water temperature influences both of these terms. In the first term, the water body receives energy through net radiation (Q^*). The water temperature represents the heat storage in the water body, which directly influences N . In the second term, the surface water temperature affects the vapour pressure gradient ($P_{vw}^* - P_v$), while the wind function determines the rate at which the water vapour is carried away.

The model created by Yao (2008) consists of two coupled parts – the first part models the atmospheric parameters over water as required by the PM equation, while the second models the temperature profile of the water body. The alteration employed for the following simulation was made only on the first part, in which wind speed profile was calculated along the wind fetch. The maximum height of the simulation was 20m and the vertical grid step (dh) was 0.5m. The total length of the simulation was 2 km, representing the wind fetch length, and the horizontal step (dx) used was 100m.

5.2.2. Wind Modelling

The evolution of the wind velocity over water is governed by the balance between horizontal convection and turbulent diffusion (Condie and Webster, 1997; Jacobson, 1999; Oke, 1978 and Weisman and Brutsaert, 1973), according to Equation 6. The evolution of the other simulated atmospheric parameters (vapour pressure and air temperature) can be found in Yao (2008).

$$u_{(h)} \frac{\partial u_{(h)}}{\partial x} = \frac{\partial}{\partial h} \left(K_M \frac{\partial u_{(h)}}{\partial h} \right) \quad (6)$$

where: $u_{(h)}$ ($\text{m}\cdot\text{s}^{-1}$) is the wind speed at height h above water and at distance x from land along wind fetch; and K_M ($\text{m}^2\cdot\text{s}^{-1}$) is the vertical eddy diffusion coefficient for momentum at h . As this equation is a non-linear partial differential equation, it is solved by Newton's iteration.

The vertical eddy diffusion coefficient (K_M) is calculated according to Monion-Obukhov similarity theory (Condie and Webster, 1997 and Jacobson, 1999):

$$K_M = \frac{\kappa u^* z}{\varphi_M} \quad (7)$$

where: κ is the von Karman constant (0.4); u^* is the friction velocity overwater (a scaling variable that represents the turbulent flux of horizontal momentum within the boundary layer); z is the height at which the vertical eddy diffusion coefficient is calculated; and φ_M is a parameter which is a function of the ratio between z and the Monin-Obukhov length, ζ (Jacobson, 1999):

$$\varphi_M = \begin{cases} 1 + \beta_M \frac{z}{\zeta}, & \text{if } \frac{z}{\zeta} > 0 \\ (1 - \gamma_M \frac{z}{\zeta})^{-0.25} & \text{if } \frac{z}{\zeta} < 0 \\ 1 & \text{if } \frac{z}{\zeta} = 0 \end{cases} \quad (8a)$$

$$\varphi_M = \begin{cases} (1 - \gamma_M \frac{z}{\zeta})^{-0.25} & \text{if } \frac{z}{\zeta} < 0 \end{cases} \quad (8b)$$

$$\varphi_M = \begin{cases} 1 & \text{if } \frac{z}{\zeta} = 0 \end{cases} \quad (8c)$$

where β_M , γ_M are empirical constants, valuing 6.0 and 19.3, respectively, when von Karman constant is 0.4; and the Monin-Obukhov length, ζ , is given by Jacobson (1999):

$$\zeta = - \frac{u^{*3} \theta_{v(z)}}{\kappa g (\overline{\varpi' \theta_v'})_z} \quad (9)$$

where: $\theta_{v(z)}$ is the air temperature over water at z height; κ is the von Karman constant; g is the gravitational acceleration; and $(\overline{\varpi' \theta_v'})_z$ is the bulk aerodynamic vertical kinematic turbulent sensible-heat flux (Jacobson, 1999). This term is calculated as follows:

$$(\overline{\varpi' \theta_v'})_z = -C_H u_{(z)} (\theta_{v(z)} - \theta_{v(z_o)}) \quad (10)$$

where: C_H is the bulk heat-transfer coefficient (0.0015); $u_{(z)}$ is the wind velocity at z height; $\theta_{v(z)}$ is the air temperature over water at z height; and $\theta_{v(z_o)}$ is the air temperature at height (z_o). The potential virtual temperature at surface $\theta_{v(0)}$ can be used for convenience instead of $\theta_{v(z_o)}$ (Jacobson, 1999).

5.2.3. Boundary Conditions

The atmospheric boundary layer in Yao (2008) is defined as the layer of air in the vicinity of a ground or water surface. The wind speed profile is described as a logarithmic function as shown in Figure 11. The wind profile is determined by the surface roughness. In woodland and urban areas, the wind in the boundary layer is impeded and the height of the boundary is greater than in smoother surfaces, such as water. This may be a source of error if land weather station data are used to estimate evaporation from open-water bodies.

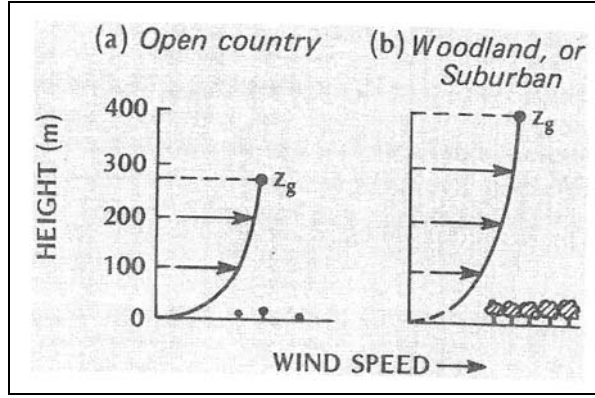


Figure 11: Examples of wind speed profiles in a boundary layer (Oke, 1978 presented by Yao, 2008)

To calculate the wind speed profile within the boundary layer for the first horizontal grid point, the model first converts the wind speed measured at the land station at 10m height to a value at 20m height according to the relationship:

$$u_{(z)} = u_{ref} \frac{\ln \frac{z}{z_{oo}}}{\ln \frac{z_{ref}}{z_{oo}}} \quad (11)$$

where: u_{ref} is a known value of wind speed measured at z_{ref} height; z_{oo} is the over land roughness length (assumed to be 0.02m); and z is the height at which the wind speed is to be calculated.

The wind speed at $z = 20$ m over land is then adjusted to a value over water as a function of the difference between the air temperature over land (T_{al}) and the surface water temperature (T_{ws}), according to Beletsky and Schwab (2001), Schwab (1978) and Schwab and Morton (1984):

$$u_{(20)} = (1.2u_{l(20)} + 1.85) \left[1 - \frac{\Delta T}{|\Delta T|} \left(\frac{|\Delta T|}{1920} \right)^{1/3} \right] \quad (12)$$

where: $u_{(20)}$ is the adjusted wind speed over water; $u_{l(20)}$ is the wind speed over land at 20m height; and $\Delta T = T_{al} - T_{ws}$ (°C).

The friction velocity over water is calculated as a function of the wind speed over water at 20m height:

$$u^* = \kappa \frac{u_{(z)}}{\ln \frac{z}{z_o}} \quad (13)$$

where: u^* is the friction velocity; κ is the von Karman constant (0.4); $u_{(z)}$ is the known wind velocity at z (in this case, at 20m height); and z_o is the over water roughness length (assumed to be 0.00004m).

By using the adjusted wind speed at 20m and the friction velocity over water, the profile of wind velocities at the first horizontal grid point is calculated by Monion-Obukhov similarity theory (Condie and Webster, 1997; Jacobson, 1999):

$$u_{(h)} = \frac{u^*}{\kappa} \left[\ln \left(\frac{z}{z_o} \right) - \psi_M \right] \quad (14)$$

where ψ_M is a parameter calculated by:

$$-\frac{\beta_M}{\zeta} (z - z_{oo}), \quad \text{if } \frac{z}{\zeta} > 0 \quad (15a)$$

$$\left\{ \begin{array}{l} \ln \left[\frac{(1 + \varphi_{M(z)}^{-2})(1 + \varphi_{M(z)}^{-1})^2}{(1 + \varphi_{M(z_{oo})}^{-2})(1 + \varphi_{M(z_{oo})}^{-1})^2} - 2 \tan^{-1} \left(\frac{1}{\varphi_{M(z)}} \right) + 2 \tan^{-1} \left(\frac{1}{\varphi_{M(z_{oo})}} \right) \right] \quad \text{if } \frac{z}{\zeta} < 0 \\ 0, \quad \text{if } \frac{z}{\zeta} = 0 \end{array} \right. \quad (15b)$$

$$\left. \begin{array}{l} \\ \end{array} \right\} \quad (15c)$$

As described earlier, the Monin-Obukhov length, ζ , is given by Equations 9 and 10, and the parameter φ_M , which is a function of the ratio between z and the Monin-Obukhov length, by Equation 8. β_M is a constant equal to 6.0 when the von Karman constant is 0.4.

5.2.4. Windbreak Effect Inclusions

Medium porosity windbreaks with heights of 20m, 30m and 40m, were simulated. In order to effectively examine the influence of these barriers on wind speed, the wind speed over water with various windbreaks was modelled along the wind fetch based on the results found by van Eimern *et al.* (1964), Bradley and Mulhearn (1983), Brandle and Finch (1991), Wang and Takle (1995a), Hipsey *et al.* (2004), and Brandle *et al.* (2004) as displayed in Figure 12.

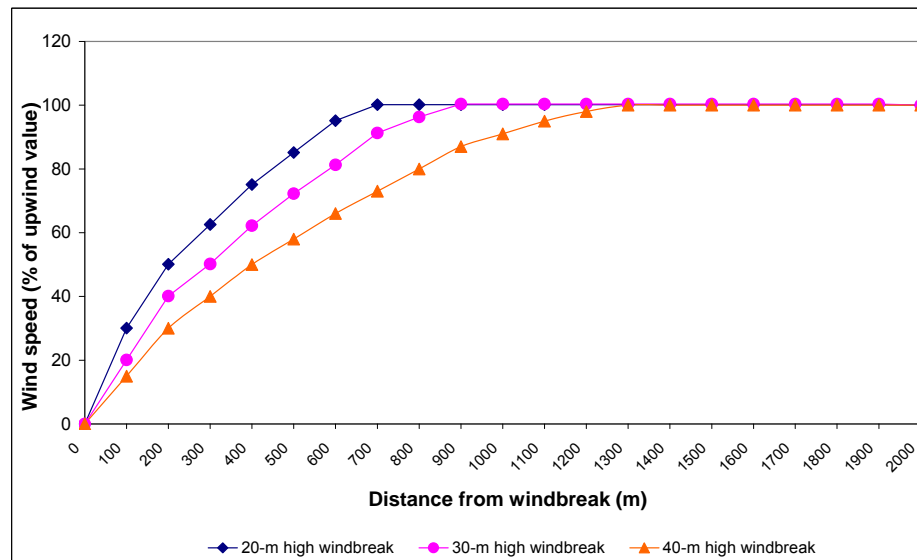


Figure 12: Horizontal profiles of wind speed on the leeward side of windbreaks with different heights (adapted from the works of van Eimern *et al.*, 1964; Bradley and Mulhearn, 1983; Brandle and Finch, 1991; Wang and Takle, 1995a; Hipsey *et al.*, 2004 and Brandle *et al.*, 2004)

It is important to note that several assumptions were made during the modelling process:

- The reductions showed in Figure 12 occurred without any vertical variation;
- The windbreaks were placed perpendicularly to the prevailing wind direction. According to the Bureau of Meteorology (2008), data from 1965 to 2008 show that the annual prevailing wind at University of Queensland Gatton station (site number 040082) is westerly. Therefore, the barriers were positioned in a south-northerly direction, on the western side of the dam, along its contour;
- The barriers were established in the immediate vicinity of the dam, so the reductions in wind speed presented in Figure 12 occur over the water (when the dam is at full supply), and not over the land; and
- The dam had an evenly distributed width of 2 km (Figure 13), an area of 100 km², and a depth of 25m.

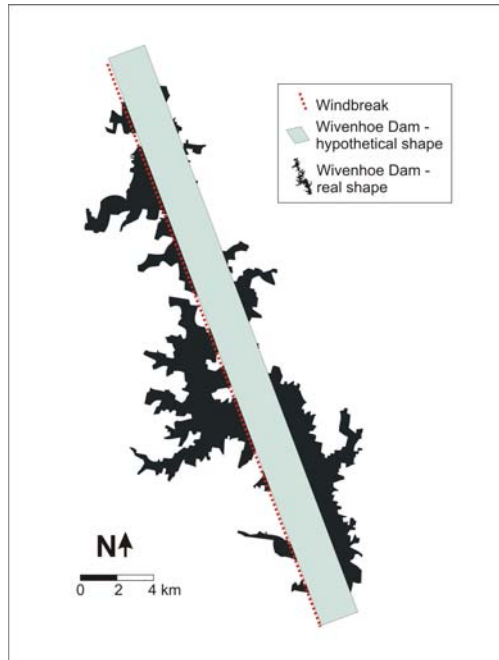


Figure 13: Hypothetical shape of Wivenhoe Dam for the simulations

6. MODELLING RESULTS

The following conventions were used to examine the simulations carried out in this study:

- Scenario 1 = no windbreak (baseline scenario);
- Scenario 2 = 20m high windbreak;
- Scenario 3 = 30m high windbreak; and
- Scenario 4 = 40m high windbreak.

The monthly evaporation rates of Wivenhoe along wind fetch in 2007 for all the four scenarios are shown in Table 1.

Table 1: Estimated monthly evaporation rates for different windbreak protection scenarios along the wind fetch¹ of Wivenhoe Dam in 2007 (mm)

	Simulation 1: No windbreak	Simulation 2: 20m high windbreak	Simulation 3: 30m high windbreak	Simulation 4: 40m high windbreak
January	144.5	138.9	136.2	131.9
February	192.0	186.8	184.3	180.2
March	193.9	189.6	187.6	184.2
April	152.4	149.7	148.3	146.2
May	116.6	114.7	113.7	112.2
June	106.0	103.3	102.0	99.9
July	87.6	85.5	84.4	82.8
August	80.5	78.7	77.8	76.5
September	120.6	116.8	115.0	112.1
October	165.1	161.0	159.1	155.8
November	175.4	171.3	169.3	166.1
December	176.4	172.7	170.9	168.0
Annual	1710.8	1669.0	1648.7	1615.9

¹Wind fetch = 2 km

Table 2 briefly summarises the seasonal results of the simulations. The simulated annual evaporation rate was calculated as 1,711mm for the baseline scenario. The annual evaporation rates for the 20m, 30m and 40m high windbreak scenarios were found to be 1,669, 1,649 and 1,616mm respectively, each representing overall reductions of 2.5, 3.6 and 5.6%. During summer, evaporation rates were reduced by 2.8, 4.2 and 6.4% respectively; and during winter by 2.4, 3.5 and 5.4% respectively. These reduction rates are relatively small compared with the evaporation reduced using other techniques like suspended covers (Yao *et al.*, 2009) and monolayers (McJannet *et al.*, 2008b). Nevertheless, the reduction of 5.6% as seen for the 40m high windbreak is still a significant saving, and as such, this technique warrants further, more detailed, investigation.

Table 2: Summary of the results of the simulations on Wivenhoe Dam during 2007

	Scenario 1: no windbreak	Scenario 2: 20m high windbreak	Scenario 3: 30m high windbreak	Scenario 4: 40m high windbreak
Annual evaporation rate (mm)	1,711	1,669	1,649	1,616
Reduction efficiency (%)	-	2.5	3.6	5.6
Summer ¹ evaporation rate (mm)	513	498	491	480
Reduction efficiency (%)	-	2.8	4.2	6.4
Winter ² evaporation rate (mm)	274	267	264	259
Reduction efficiency (%)	-	2.4	3.5	5.4

¹ Summer = December, January and February ² Winter = June, July and August

Figure 14 shows the annual evaporation rates over the wind fetch (2 km) for each scenario. Over a distance of up to 200m behind the barrier, annual evaporation rates for the 20, 30 and 40m high windbreaks were calculated as being 85, 81.6 and 78.5% (respectively) of the baseline evaporation level. Over a distance of 1 km, annual evaporation rates were found to be 95.1, 92.7 and 89.2% (respectively) of the baseline value. Finally, when considering the entire dam width, the simulations showed that evaporation was 97.5, 96.4 and 94.4% (respectively) of the baseline rate.

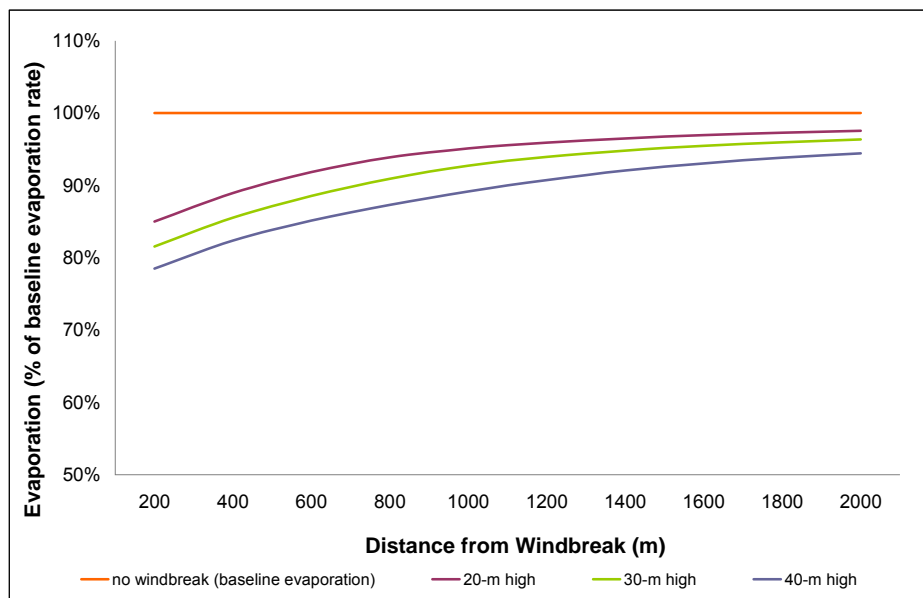


Figure 14: Calculated annual evaporation rate on the leeward side of windbreaks with different heights at Wivenhoe Dam in 2007

Figure 15 shows the annual wind speed reduction along the wind fetch of Wivenhoe Dam in 2007 for all scenarios simulated in this study. The percentages of wind speed for the windbreak scenarios are cumulative and represent the total reduction in velocity expected over each accumulated distance behind the barrier, up to a distance of 2 km (the width of Wivenhoe Dam). Over the first 200m, wind speed was found to be reduced by 21, 29 and 39% of the baseline wind speed for the windbreak

heights of 40, 30 and 20m respectively. Wind gradually recovers its open velocity and reaches open values at distances of 600, 800 and 1,200m behind the barrier. The average effect of windbreaks on wind reduction over the entire 2 km distance was 89.4, 84.7 and 77% (respectively) of the open values.

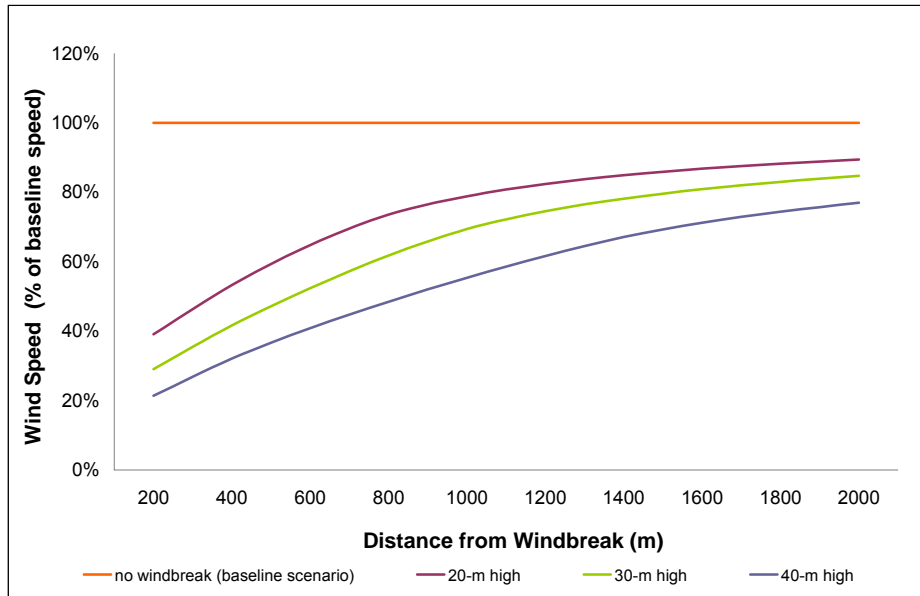


Figure 15: Estimated annual wind speed reductions on the leeward side of windbreaks with different heights at Wivenhoe Dam in 2007

The simulations of the scenarios with windbreaks displayed lower evaporation rates, making it clear the wind speed reduction caused by the presence of a barrier can lead to a decrease in the loss of water. However, evaporation reductions due to the presence of tree belts were not proportional to reductions in wind speed. While wind speed was reduced by 10.6, 15.3 and 23% when 20, 30 and 40m high windbreaks were used, the annual evaporation rate was reduced by only 2.5, 3.6 and 5.6% respectively. These results show that incoming solar radiation is potentially the main driving force behind the evaporation process in Wivenhoe Dam. When the dam is 100% covered with suspended or floating covers to reduce energy input, evaporation is expected to be reduced by 68 to 76%, depending on the cover material (Yao et al., 2009).

It is also important to note that the effectiveness of windbreaks in reducing evaporation is highly dependent upon water level. The results of this study are valid only if windbreaks are placed by the edge of the dam, the dam is at full supply level, and the wind blows perpendicularly to the windbreak line. For any scenario different from that, smaller evaporation reductions are expected. Additionally, because Wivenhoe is a natural dam with gently sloping sides, any small variations in water level would allow for large differences to develop in the distance between the water and windbreak, which is the key factor in determining the effectiveness of the barrier in reducing evaporation. This reasoning is why windbreaks have been recommended for small and steep-sided dams (Hypsey, 2002; Hipsey *et al.*, 2004; Watts, 2005), and not larger dams.

7. COST EFFICIENCY

Wivenhoe Dam is not always operating at full supply level, and as it is a low profile type dam, any small variation in water level lead to a sizeable variation in total surface area. For example, if the surface area is reduced to 60% of that expected at full supply, the new distance between water and windbreak will result in annual evaporation levels from the dam being reduced by only 1.1, 2.0 and 3.8% for the 20, 30 and 40m high windbreaks (respectively) when compared with the rate of natural evaporation. Based on this, a cost efficiency study on the use of barriers along the reservoir was not carried out.

8. KEY MESSAGES

- The effect of windbreaks on evaporation will be highly dependent upon the dam's shape and side gradient.
- Windbreaks positioned near the water will have more effect on evaporation reduction, as wind speed is reduced at higher levels in their close vicinity. For this reason, narrow, steep-sided dams, with length positioned perpendicularly to the prevailing wind, will experience higher levels of evaporation reduction than wide dams with low sloping sides.
- The efficiency of windbreaks in reducing wind speed, and thus evaporation, depends upon their porosity and height. Higher evaporation reduction levels will be expected for higher windbreaks, as wind speed is reduced proportionally to the height of the barrier.
- Windbreaks have a strong effect on wind reduction only in the very close vicinity of the barrier, which extends downwind up to 5 H. Therefore, given the difficulties in achieving a large windbreak height to dam-fetch ratio, it is unlikely that windbreaks will be widespread methods for evaporation reduction on large dams (Watts, 2005).
- If trees are to be used as windbreaks, it must be considered that the planting of trees around water storage may increase the risk of piping failure (Department of Natural Resources and Mines, 2003) and additional water loss through evapotranspiration, which will have to be subtracted from whatever evaporation savings may result (Frenkiel, 1965). Additionally, issues such as growing time, hazard to dam integrity and impacts on water quality require consideration.
- It is important to note the spatial pattern of evaporation cannot be diagnosed solely on the basis of the horizontal wind speed reduction. Turbulent flux is also important, as it indicates the possible transport of water vapour and thus the evaporation flux extending downwind of the windbreak (Cleugh, 1998; Cleugh, 2002). In this initial study, turbulent flux variations due to the presence of windbreaks was not considered as the effect of windbreaks on turbulence is not well known (Wang *et al.* 2001).
- Turbulence should be considered especially because the wake zone, which extends from about 10 to 30 H, is considered a zone of intense turbulence, where wind is recovering its velocity and the turbulent air prevents the accumulation of moisture above or near the surface of the water (Raine and Stevenson, 1977; Hipsey, 2002). Therefore, this zone is believed to experience even greater loss of water due to evaporation. According to the reviews of McNaughton (1988), the turbulent transport of heat and vapour is reduced within the quiet zone and enhanced within the wake zone.

9. CONCLUSION

This study addressed the potential for windbreaks to reduce evaporation from water storages in SEQ using desktop modelling. A narrow dam, assumed to be at full supply, was chosen as a case study. In this analysis, the most efficient windbreak density in reducing wind speed was considered, and a range of heights (varying from 20 to 40m) were tested. Windbreaks were placed parallel to the length of the dam, and wind direction was set to constantly blow perpendicularly to the windbreak line. With these features, an optimum scenario was composed and evaporation reductions maximised.

The results showed that reductions in annual evaporation levels of only 2.5, 3.6 and 5.6% can be achieved for 20, 30 and 40m high windbreaks respectively. These percentages were estimated to be even smaller, at 1.1, 2.0 and 3.8% at 60% of the full supply.

Despite strong recommendation that windbreaks will reduce evaporation from small farm dams (Hipsey, 2002; Hipsey *et al.*, 2004), the simulations carried out in this study and the results from other researchers show that even under optimal conditions, only minor reductions in evaporation rates can be expected for large dams.

REFERENCES

- Beletsky, D. and Schwab, D.J. 2001. Modelling circulation and thermal structure in Lake Michigan: Annual cycle and interannual variability. *Journal of Geophysical Research*, 106: 19745-19771.
- Bradley, E.F. and Mulhearn, P.J. 1983. Development of velocity and shear stress distributions in the wake of a porous shelter fence. *J Wind Eng Ind Aerodyn*, 15: 145-156.
- Brandle, J.R. and Finch, S. 1991. How Windbreaks Work, University of Nebraska Cooperative Extension EC 91-1763-B.
- Brandle, J.R., Hodges, L. and Zhou, X.H. 2004. Windbreaks in North American Agricultural Systems. *Agroforestry Systems*, 61: 65-78.
- Brown, K.W. and Rosenberg, N.J. 1971. Shelter-effects on microclimate, growth and water use by irrigated sugar beets in the great plains. *Agric. Meteorol.* 9: 241-263.
- Bureau of Meteorology, 2003. Climate Statistics for Australian Locations, Bureau of Meteorology, Canberra, viewed 2 December 2008, http://www.bom.gov.au/climate/averages/tables/cw_040082.shtml
- Calder, I.R. and Neal, C. 1984. Evaporation from saline lakes: a combination equation approach. *Hydrol. Sciences J.* 29: 89-97.
- Cleugh, H.A. 1998. Effects of windbreaks on airflow, microclimates and crop yields. *Agroforestry Systems*, 41: 55-84.
- Cleugh, H.A. 2002. Field measurements of windbreak effects on airflow, turbulent exchanges and microclimates. *Australian Journal of Experimental Agriculture*, 42: 665-677.
- Cleugh, H.A., Prinsley, R., Bird, R., Brooks, S.J., Carberry, P., Crawford, M., Jackson, T., Meinke, H., Mylius, S., Nuberg, I., Sudmeyer, R. and Wright, A. 2002. The Australian National Windbreaks Program: overview and summary of results. *Australian Journal of Experimental Agriculture*, 42: 649-664.
- Condie, S.A. and Webster, I.T. 1995. Evaporation Mitigation from on-Farm Water Storages. CSIRO, Canberra.
- Condie, S.A. and Webster, I.T. 1997. The influence of wind stress, temperature and humidity gradients on evaporation from reservoirs. *Water Resources Research*, 33: 2813-2822.
- Department of Natural Resources and Mines. 2003. Methods for Reducing Evaporation from Storages used for Urban Water Supplies. GHD.
- Finnigan, J.J. and Bradley, E.F. 1983. The turbulent kinetic energy budget behind a porous barrier: an analysis in streamline co-ordinates. *J. Wind Eng. Ind. Aerodyn.*, 15: 157-168.
- Food and Agriculture Organization of the United Nations (FAO). 1989. Arid Zone Forestry: a Guide for Field Technicians. FAO Conservation Guide No. 20. FAO, Rome, viewed 11 November 2008, <http://www.fao.org/docrep/t0122e/t0122e0a.htm>
- Frenkiel, J. 1965. Evaporation Reduction: Physical and Chemical Principles and Review of Experiments. UNESCO: Paris.
- Heisler, G.M. and Dewalle, D.R. 1988. Effects of windbreak structure on wind flow. *Agric. Ecosyst. Environ.* 22-23:41-69.
- Hipsey, M. 2002. Using windbreaks to reduce evaporation from farm dams, Department of Agriculture WA, Farmnote 72/2002, viewed 20 July 2008, http://www.agric.wa.gov.au/content/1we/water/watstor/fn072_2002.pdf
- Hipsey, M.R. and Sivapalan, M. 2003. Parameterizing the effect of a wind shelter on evaporation from small water bodies. *Water Resour. Res.*, 39: 1-9.
- Hipsey, M.R., Sivapalan, M. and Clement, T.P. 2004. A numerical and field investigation of surface heat fluxes from small wind-sheltered waterbodies in semi-arid Western Australia. *Environ. Fluid Mech.*, 4:79-106.
- Jacobson, M.Z. 1999. Fundamentals of Atmospheric Modelling. Cambridge: Cambridge University Press.
- Jensen, M. E., Burman, R. D. and Allen, R. G. 1990. Evapotranspiration and Irrigation Water Requirements. New York: American Society of Civil Engineers, Manuals and Reports on Engineering Practice No. 70.
- Judd, T.S., Attiwill P.M. and Adams M.A, 1996. Nutrient concentrations in Eucalyptus: a synthesis in relation to differences between taxa sites and components. In: Nutrition of eucalypts, eds. PM Attiwill, MA Adams) CSIRO Publishing.
- Lomas, J. and Schlesinger, E. 1971. The influence of a windbreak on evaporation. *Agric. Meteorol.* 8: 107-115.
- Messing, I., Afors, M., Radkvist, K. and Lewan, E. 1998. Influence of shelterbelt type on potential evaporation in an arid environment. *Arid Soil Res. Rehab.* 12: 123-138.

- Miller, D. R., Rosenberg, N.J. and Bagley, W.T. 1973. Soybean water use in the shelter of a slat-fence windbreak. *Agric. Meteorol.* 56: 209-25.
- McNaughton, K.G. 1988. Effects of windbreaks on turbulent transport and microclimate. *Agriculture, Ecosystems and Environment*, 22/23: 17-39.
- McJannet, D., Webster, I.T. and Cook, F.J. 2008a. An evaporation wind function for open water bodies of variable size. *Water Resources Research*, Submitted.
- McJannet, D., Cook, F., Knight, J. and Burn, S. 2008b. Evaporation Reduction by Monolayers: Overview, Modelling and Effectiveness. CSIRO: Water for a Healthy Country National Research Flagship.
- Monteith, J. L. 1965. Evaporation and the environment. In *The State and Movement of Water in Living Organisms* (G.E. Fogg, ed). London: Cambridge University Press.
- Oke, T.R. 1978. *Boundary Layer Climates*. London: Methuen and Co Ltd.
- Pryor, D. and Nadler, A. 2006. Examining micro-climate effects in field crop production, Proceedings of the 7th Annual Manitoba Agronomists Conference, Manitoba, viewed 15 August 2008, http://proxycheck.lib.umanitoba.ca/afs/agronomists_conf/proceedings/2006/nadler_pryor_examining_micro_climate.pdf
- Raine, J.K. and Stevenson, D.C. 1977. Wind protection by model fences in a simulated atmospheric boundary layer. *J. Indust. Aerodyn.*, 2: 159-180.
- Rosenberg, N.J. 1966. Microclimate, air mixing and physiological regulation of transpiration as influenced by wind shelter in an irrigated bean field. *Agric. Meteorol.* 3: 197-224.
- Skidmore, E.L. and Hagen, L.J. 1970. Evaporation in sheltered areas as influenced by windbreak porosity. *Agric. Meteorol.*, 7: 363-374.
- Schwab, D.J. 1978. Simulation and forecasting of Lake Erie storm surges. *Monthly Weather Review*, 106: 1476-1487.
- Schwab, D.J. and Morton, J.A. 1984. Estimation of overlake wind speed from overland wind speed: a comparison of three methods. *Journal of Great Lakes Research*, 10: 68-72.
- Sudmeyer, R.A. and Scott, P.R. 2002. Characterisation of a windbreak system on the south coast of Western Australia. 1. Microclimate and wind erosion. *Australian Journal of Experimental Agriculture*, 42: 703-715.
- van Eimern, J., Karshon, R., Razumova, L.A. and Robertson, G.W. 1964. Windbreaks and Shelterbelts. *World Meteorol. Org. Technical Note No. 59*.
- Wang, H. and Takle, E.S. 1995a. Numerical simulations of shelterbelt effects on wind direction. *Boundary-Layer Meteorol.*, 75: 141-173.
- Wang, H. and Takle, E.S. 1995b. A numerical simulation of boundary-layer flow near shelterbelts. *J. Appl. Meteor.*, 34: 2206-2219.
- Wang, H. and Takle, E.S. 1997a. Momentum budget and shelter mechanism of boundary layer flow near a shelterbelt. *Boundary-Layer Meteorol*, 82: 417-435.
- Wang, H. and Takle, E.S. 1997b. Model-simulated influences of shelterbelt shape on wind-sheltering efficiency. *Journal of Applied Meteorology*, 36: 695-704.
- Wang, H. and Takle, E.S. 1998. Agricultural shelterbelts protection functions. *ASAE Annu. Int. Meet.*, Orlando, FL, pp. 36. St Joseph, Mich.: ASAE.
- Wang, H., Takle, A and Shen, J. 2001. Shelterbelts and Windbreaks: mathematical modelling and computer simulations of turbulent flows. *Annu. Rev. Fluid Mech.*, 33: 549-86.
- Watts, P.J. 2005. Scoping Study – Reduction of Evaporation from Farm Dams. Final report to the National Program for Sustainable Irrigation. Feedlot Services Australia Pty Ltd, Toowoomba.
- Weisman, R.N. and Brutsaert, W. 1973. Evaporation and cooling of a lake under unstable atmospheric conditions. *Water Resources Research*, 9: 1242-1257.
- Wilson, J.S. and Josiah, S.J. 2004. *Windbreak Design*, Institute of Agriculture and Natural Resources, University of Nebraska – Lincoln Extension, NebGuide G1304, viewed 20 July 2008, <http://www.nfs.unl.edu/documents/windbreakdesign.pdf>
- Yao, X. 2008. An Improved 2-D Numeric Model for Open-Water Daily Evaporation Estimation. BSc Thesis, Griffith University.
- Yao, X., Zhang, H. and Lemckert, C. 2009. Evaporation Reduction by Suspended and Floating Covers: Overview, Modelling and Efficiency. CSIRO: Water for a Healthy Country National Research Flagship.

Urban Water Security Research Alliance

